Al-Khwarizmi Engineering Journal, Vol. 11, No. 1, P.P. 93- 112 (2015)

Al-Khwarizmi Engineering Journal

The Effect of Soil Content, Drilling Parameters and Drilling Tool Diameter on the Vibration Assessment in the Drilling Rig

Mauwafak Ali Tawfik* **Wafa Abd Soud****
Rami Safaa Alwan***
*,**,*** *Department of Mechanical Engineering / University of Technology*
E-mail: drmat19853@yahoo.com
E-mail: wafaabd_92@yahoo.com
E-mail: rami.safaa@yahoo.com

(Received 8 April 2014; accepted 15 December 2014)

Abstract

This paper represents a study of the effect of the soil type, the drilling parameters and the drilling tool properties on the dynamic vibrational behavior of the drilling rig and its assessment in the drilling system. So first, an experimental drilling rig was designed and constructed to embrace the numerical work.

The experimental work included implementation of the drill-string in different types of soil with different properties according to the difference in the grains size, at different rotational speeds (RPM), and different weights on bit (WOB) (Thrust force), in a way that allows establishing the charts that correlate the vibration acceleration, the rate of penetration (ROP), and the power consumption curves with the depth of drilling.

In addition to that the ANSYS Workbench (the 14.0 release) software was used to simulate and verify the experimental results. And it was also used to model other numerical cases with different drill bit diameters.

Keywords: *Soil, Vibration, and Drilling Rig.*

1. Literature Survey

In 2000 Tucker and Wang were motivated by the need to understand the complex vibrational states experienced by the active components of a drilling assembly, in order to better control their potential [1]. In 2001 Ashley et al. dealt with the application of the multi-axis vibration chassis (MVC) to measure vibrations in multiple axes and using the achieved data to provide the drilling team with the necessary means to control the proper parameters to minimize specific vibration effects [2]. In 2002 Gui et al. studied the subject of instrumented borehole drilling and using the achieved data from the measured parameters as a tool in subsurface investigation [3]. In 2002 Leine et al. attempted to explain the complicated behavior of oil well drillstring motion when both torsional stick-slip and lateral whirl vibration are involved [4]. In 2004 Hendriks had focused on the analysis of torsional vibrations, lateral vibrations and the interaction between those vibrations in specific experimental drill string set-up [5]. In 2005 Mihajlovic had focused on the separate analysis of friction-induced vibrations in flexible mechanical systems and lateral vibrations in rotor systems due to mass-unbalance [6]. In 2006 Piovan and Sampio presented a continuous model to study, by means of finite element discretization, the coupling of extensional, flexural and torsional vibration on a drill string [7]. In 2009 Moradi et al. modeled the drill string as a cantilever Euler-Bernoulli beam, and a tunable vibration absorber (TVA), as a semi active controller, was designed to suppress the forced bending (transverse) vibration during the drilling process [8]. In 2010 Ritto analyzed nonlinear dynamics of the drill-string which included uncertainty modeling [9]. In 2011 Liao had studied the drill-string dynamics through combined experimental, modeling and

numerical effort [10]. In 2012 Rajnauth had focused on reducing the torsional vibration as a result of monitoring and implementing corrective actions [11]. In 2013 Richard Duff proposed an improved physical laboratory model to explore dynamic behaviors associated with vibration, where the model included contact with the borehole wall allowing a range of stabilization geometries while removing bit-formation interaction effects [12].

From the previously published works and papers it was observed that many drilling vibration associated problems were taken into consideration throughout the past years. These problems included the following:

- Studying drill-string dynamics.
- The effect of non-linearities.
- The vibrational behavior states.
- Utilizing measured drilling parameters data as an investigation tool.
- Vibration analysis.
- Vibration monitoring and control systems.
- Bit and bearings design.
- Finding new ways to model and analyze vibration.

So this work can be considered as a first step towards the connecting link in the previously mentioned topics chain.

2. Aims of the Work

The main aims of this work were:

1. Designing and constructing an experimental drilling rig.
2. Studying the effect of different soil types on the drilling rig vibration assessment and the rate of penetration (ROP).
3. Studying the effect of drilling parameters (rotational speed & WOB) on the vibration assessment and the (ROP).
4. Studying the effect of the drill-bit size (diameter) on the drilling rig vibration assessment.

3. The Experimental Drilling Rig

For the sake of the experimental work an experimental drilling rig was designed and construct as shown in Figure (1), which also can be tuned easily to work as a field drilling rig thanks to its adjustable height due to its removable extension legs.

Fig. 1. The experimental drilling rig.

The drilling rig basically consists of three main parts:

- The Drill-String (Drilling Core).
- The Electrical Motor and the Inverter.
- The Chassis (Frame).

(Details of the experimental rig are shown in appendix (**A**)).

The drill-string represents the mechanical part of the system, and in general its function is to receive and transmit the Weight on bit WOB (Thrust force) and the rotational movement to the drill bit, so that the downhole drilling action by the drill bit can take place.

The electrical motor and the inverter can be characterized as the electronic part of the experimental drilling rig system, and it's the one responsible of generating the rotational motion and the torque (drilling energy) and controlling them.

The chassis is made of angle iron welded to iron legs. the legs can be extended by adding the extension legs, where the rig is designed in a way that allows us to work on two levels, the first level is for field drilling which can be achieved by abandoning the extension legs, while the second level is for experimental drilling (i.e. drilling in a mold or a container) which can be achieved by adding the extension legs.

4. Instruments

Throughout the experimental work it was essential to measure and record the vibration acceleration, the power consumption, and the rate of penetration (ROP), and in order to achieve that piezoelectric charge accelerometers (B&K 4370) were used to measure vibration acceleration which was connected to a charge amplifier (B&K 2635) which was in turn connected to an oscilloscope

(ADS 1022C) to present the output signal. (See appendix D)

Also an Inverter (Hyundai N100^{plus}/015SF) was implemented to control the frequency of the electricity and in turn control the rotational speed of the motor.

For measuring the rate of penetration (ROP) a simple mechanism was used which is illustrated in Fig. (2). It consists of a slide bush (part (a)) with an adjustable-length pin (part (b)), and as the drill-string proceeds forehead during the drilling process the pin will be pushed downward with it by the upper slide bush (part (c)), the pin is in turn pointed to a ruler (part (d)) to measure the depth.

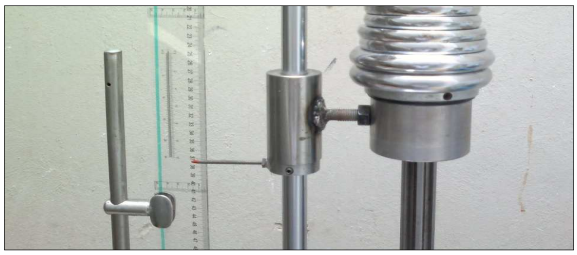

Fig. 2. Rate of penetration (ROP) measuring mechanism.

5. Soil Samples Analysis

For the sake of the experimental work three different soil samples were selected, these samples were then taken to the soil laboratory to examine their texture by performing the following procedure: the first step was to dry each soil sample in the drying oven for (24 hours) to assure that the measured mass is of the soil only (i.e. purely soil without moisture), after that (500 gram) were taken from each sample and washed with water on the No. 200 sieve (75 µm opening size) to primarily separate each sample into coarse grains portion and fine grained one. Later and after drying each portion for another (24 hours) and to be capable of finding out the grains size distribution of each sample a set of sieves was used for the coarse grained portion (grain size > 75 µm), and for the fine grained portion (grain size < 75 µm) the hydrometer analysis was used.

6. Theory of the Drill- String

In general vibration whether it was free or forced vibration, whether harmonic, periodic or random, it is basically defined as the oscillatory movement of a body about its equilibrium position. Hereby in this work the vibration in the experimental drilling rig is resulting from the Borehole-Drill bit interaction. Where the non-homogeneity of the soil results in variable drag forces on the drill-bit head, in addition to the contrastive friction forces between the conveyer and the borehole wall.

6.1. The Drill- String Model

Let us consider the drill-string as an initially straight slender rotating beam with a circular cross-section (R) and length (L) in the un-deformed state. The beam is referred to an inertial Cartesian system *O:XYZ* fixed to the undeformed beam. Another Cartesian reference system *O:xyz* measures the deformation and displacements of the beam. In Figure (3) it is possible to see that the system O:xyz is rotated with respect to the system O:XYZ by means of a typical sequence of rotation angles as usual in rotor-dynamics.

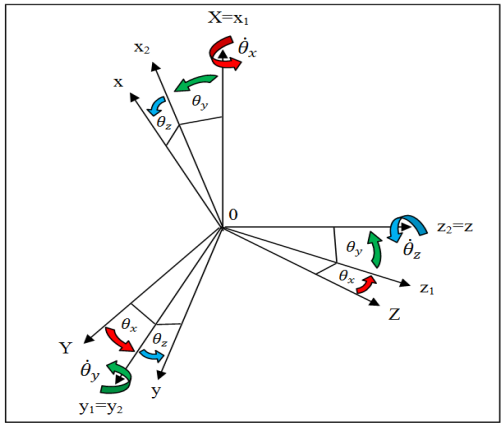

Fig. 3. Reference systems and rotation angels.

6.2. Kinetic and Strain Energies

The kinetic energy can be expressed in the following form [19]:

$$K = 0.5 \int_0^L [\rho A\,(\dot{u}^2 + \dot{v}^2 + \dot{w}^2) + \rho I(\dot{v}'^2 + \dot{w}'^2) + \rho I_0 \dot{\theta}_x^2 + 2\rho I_0 \dot{\theta}_x \dot{v}' w']\, dx \quad \ldots(1)$$

The simplified expression of the strain energy (H), which will be (H_s), can be described in the following form [19]:

$$H_s = 0.5 \int_0^L \{EAu'^2 + EI\,(v''^2 + w''^2) + GI_0\theta_x'^2\}\, dx + 0.5 \int_0^L \{GI_0\,(v''w' - v'w'')\theta_x' + EA\,(u'^3 + u'v'^2 + u'w'^2)\}\, dx + 0.5 \int_0^L \{EI_0\,(v'w'' - v''w' + \theta_x' u')\theta_x' + 3EIu'(v''^2 + w''^2)\}\, dx \quad \ldots(2)$$

The beam is subjected to its own weight, and the external work done by a vertical force due to gravity field can be expressed as [20]:

$$W = \int_0^L (\rho g A) u \, dx \qquad \ldots(3)$$

6.3. The Numerical Analysis

In order to complete the requirements of the numerical analysis which are the drill-string geometry, the boundary conditions including the supports stiffness values (foundation stiffness* (N/m^3)), and the loads, the following route was taken which starts with using the AutoCAD 2009 software to achieve the geometry.

Then to calculate the supports stiffness values, Beam Deflection formula was used, and the detailed calculations are as follows:

1) the values of the supports reaction forces were calculated as shown in Figure (4) by adapting Beam Deflection formula:

$$y_1 = \frac{Fabc\,(L+a)}{6EI_1L} \quad and \quad y_2 = \frac{R_2bx}{6EIL}(L^2 - x^2 - b^2)$$

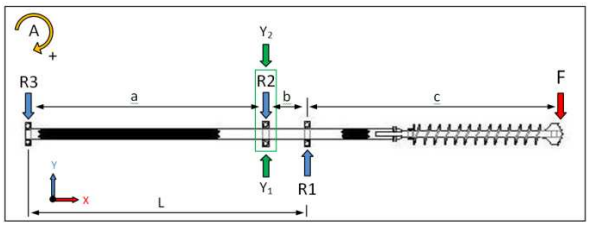

Fig. 4. The drill-string free-body-diagram.

F = obstruction and friction forces to the bit inserts and bit head surface respectively. (N)
R = Supports reactions. (N)
Y = Supports deflection. (m)
E = Young's modulus. (Pa)
I = Area moment on inertia. (m^4)

Since the summation of deflection at the supports location is equal to zero, so the value of (R_2) can be found (assuming rigid supports).

Then by taking the summation of moment about (A), then the summation of forces, the values of $(R_1)\,and\,(R_3)$ will be obtained respectively.

2) The accelerometers were then attached to the location of the supports, each one at a time, so that the displacement of each support can be found and in turn its stiffness value (K).

And finally comes the loads which were calculated as follow; at the beginning the power consumption curves for the experimental cases that have been achieved and for the free-run (idle run) (i.e. drilling with no contact between the drilling tool and the soil) were established, where the difference between the average values for the steady-state portion of them represents the drilling power consumption. And thus the loads were calculated as follows:

$$Power\ (P) = Torque\ (T) * Angular\ velocity\ (\omega) \qquad \ldots(4)$$

$$P = Power_{Free-Run} - Power_{During\ Drilling} \qquad \ldots(a)$$

$$\omega = 2\pi(N)/60 \qquad \ldots(b)$$

And according to the previous equations the only unknown value is that of (T) and by calculating it, the value of (F) for the experimental cases will be found as follows:

$$\sum T = \sum F * r_{Bit-Inserts} \qquad \ldots(c)$$

Boundary conditions

- At the supports position, radial deflection is constrained while axial translation about the drill string axis is permitted.
- The drill-bit, the drill-string and the bearings are made of elastic homogeneous isotropic steel.
- The soil stiffness is so small compared to the supports, and thus it was replaced by very low stiffness spring.

Finally and after having all the analysis requirements (geometry, boundary conditions and loads) the simulation of the original drill bit model size was available to verify the experimental results, where Figure (5 and 6) shows the undeformed and deformed model of the drill-string.

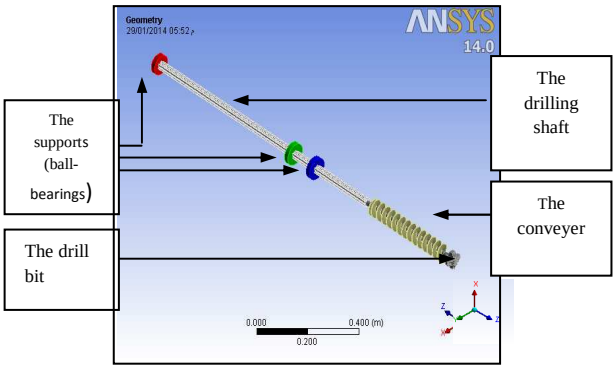

Fig. 5. ANSYS undeformed model

* Foundation Stiffness is the stiffness per the supports projected area

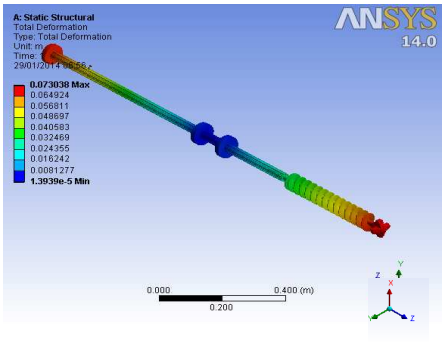

Fig. 6. ANSYS deformed model.

6.3.1. The Drill-String Natural Frequencies

Since the drilling parameters, including the drill-string rotational speed, effect on the vibration assessment had been studied in this work, so the ANSYS Workbench were used to find the drill-string natural frequencies, to make sure that the implemented operating rotational speeds that had been chosen in the experimental work are away from the natural frequencies, and in turn the achieved results are away from the effect of resonance. The results for the drill-string natural frequencies that were obtained from the ANSYS Workbench are as shown in Table (1) below:

Table 1,
The drill-string natural frequencies.

Depth (cm)	The Natural Frequencies (r.p.m.)			
	1st	2nd	3rd	4th
0	0.06	9	10	310
2	0.07	9.04	10.63	310.61
4	0.07	9.12	10.22	330.32
6	9.03	10.75	313.25	----
8	9.05	10.66	314.21	----
10	9.07	10.67	311.42	----
12	0.07	9.37	11.35	326.21
14	0.06	9.48	11.84	333.21
16	9.32	10.64	11.24	315.87
18	9.47	10.85	13.45	329.47
20	10.1	13.9	323.2	----
22	0.05	9.37	10.35	318.18
24	0.03	9.47	10.78	332.21
26	9.64	10.78	13.25	331.77
28	0.08	9.34	11.87	321.42
30	9.26	10.81	319.47	----
32	9.42	10.63	320.54	----
34	0.05	9.21	13.98	310.25
36	0.08	9.54	10.27	324.27
38	9.32	10.88	314.87	----
40	0.02	9.84	11.05	325.09

6.3.2. The Drill-Bit Diameter Effect

Additionally, the ANSYS Workbench software was used to model other numerical cases with different drill-bit size (diameter) which are ($\mp$ 25%) of the original drill bit model geometry size (diameter) to verify the effect of the drill bit size (diameter) on the vibration assessment and the results are as shown in Figure (7) below:

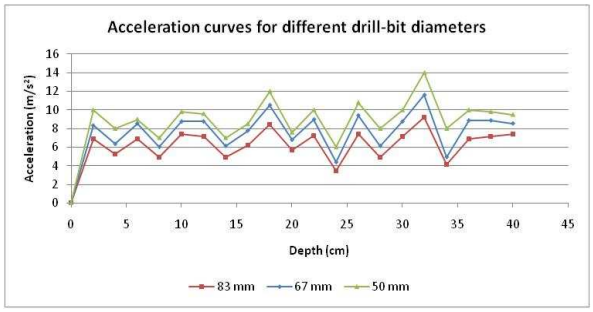

Fig. 7. Acceleration curves for different diameters.

It was observed that for the same conditions (soil type, rotational speed and weight on bit) the smaller the drill bit is, the higher the vibration acceleration levels will be, and this may be attributed either to difference in mass and in turn the difference in inertia, the fact that the larger model mass works on dissipating the transferred vibrations more than the smaller model does or other dynamical behaviors where this point needs more investigation (provided that the drill-string rotational speed is away from resonance zones).

7. Results and Discussion

For the sake of the experimental work the following parameters were chosen: three different samples of soil with different grain sizes, four different rotational speeds (50 – 100 – 150 – 200) rpm so that the rotational speed increases by folds and three weights on bit (WOB/Thrust force) with (50%) increment steps as follows (80 – 120 – 160) N. In addition to that and by using the ANSYS software it was available to simulate the original drill bit for the experimental cases that were accomplished for the purposes of verification, and further more the ANSYS software was used to model other theoretical cases with different drill bit model sizes (diameters) which are ($\pm$ 25%) of the original drill bit model size (diameter).

7.1. Soil Samples Grains Size Distribution

When it comes to vibration assessment and its severity, it turns out that they are clearly affected by the grains size distribution of the soil and the consistency of that distribution. Figure (8) below shows the grains size distribution curves of the soil samples, where x-axis represents the grains size, and y-axis represents the percentage of the grains.

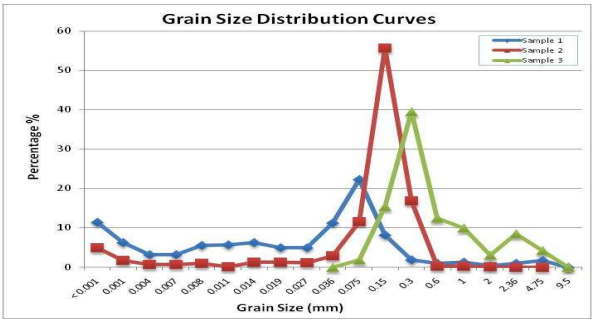

Fig. 8. Grains size distribution curves.

7.2. The Experimental Results

After finishing the soil samples analysis and the establishment of the grains size distribution curves, it was commenced with the experiments, and down hereby the obtained results, for each soil sample, are presented as follows:

7.2.1. Silty-Clay

For first soil sample (Silty-Clay), the average values of the vibration acceleration levels (m/s^2) from Figure (9, 12, and 15) were as in table (1) in Appendix (**B**).

Based on the revealed data, it can be said that vibration acceleration levels increase as the rotational speed increases. This can be attributed to the fact that external forces (that the soil exerts on the drill-bit whether they were obstruction forces to the rotation of the inserts or friction ones to the surface of the drill-bit head) which once were with little or no effect, now they do since (ω) had increased. Which eventually means that the time stepping of the forces exertion is now became less, and that is make the drill string exposed to the effect of more forces, and by that the drill string will be displaced more distance than before. That brings up the conclusion that the second reason for that increment in vibration acceleration is when the external forces shake the drill string out of its rotation axis center an imbalance force due to imbalance mass will be generated.

According to imbalance force law it appears that (ω) is the factor of the biggest impact. So increasing (ω) will greatly increase the centripetal forces and in turn the vibration levels as well (provided that the system is away from the critical rotational speeds).

It can be noticed that vibration acceleration levels decrease as the (WOB) increases due to the fact that the higher the (WOB) is, the higher the friction between the drill bit and the soil. So in other words, there will be more power dissipation in overcoming friction rather than in vibration, and of course higher friction means more reduction in the rotational speed, which in turn means lower vibration acceleration (according to the relation that was first drawn between the vibration and the rotational speed). Not only that but also more importantly is that increasing the (WOB) will diminish the effect of the external forces on the drill bit since now they will have to shake larger mass than before.

In general the vibration acceleration levels were neither too high nor too low. The most likely explanation for this behavior can be attributed to the following factors, which are the grains size distribution and the homogeneity of that distribution (i.e. the larger the grains size and the more non-homogeneity that the soil have, the higher the vibration acceleration levels that will be encountered in it).

The vibration acceleration levels decrement increases as the (WOB) and the rotational speed increase. This observations can be attributed to the fact that forces that became effective in disturbing the drill string and shaking it out of its rotation center, as the rotational speed increased (i.e. the load stepping time was reduced), are more liable to dissipation due to increment in the (WOB).

The average values of the rate of penetration (ROP) (cm/sec) from Figure (10, 13, and 16) were as in table (2) in Appendix (**B**).

In reference to table (5), it can be stated that higher rotational speed results in higher rates of penetration (ROP), since more excavation of the soil will be done.

The rate of penetration (ROP) is seemed to be affected by the (WOB) in the same way that it did by the rotational speed and the higher the (WOB) is, the higher the (ROP) will be, but that's not completely practical due to the fact that (ROP) will keep increasing with the (WOB) up to a certain point, namely the founder point. After that point increasing the (WOB) will have adverse effect on the (ROP), because the drill bit will have

more difficulty in overcoming increased friction, in addition to the fact that excessive (WOB) will force the inserts of the drill bit deeply in the formation in a way that they can't be moved properly.

It is worthy to mention that the silty-clay soil has low rate of penetration. That's because the silty-clay soil grains were sticking to the drill bit inserts causing less efficient drilling and that if they don't even make the drill bit clog which agrees with what came in reference [3]. And again this can be attributed to the grains size, because of the fact that the soil grains are generally under the influence of two main kinds of forces which are the gravitational and the surface forces, and the factor that designate the dominant force is the ratio of the surface area to the volume, so that the dominant force for the fine-grained soil will be the surface force and vice versa. And that what makes the silty-clay soil grains sticky.

The rate of penetration (ROP) increment increases as the (WOB) and the rotational speed increase. This observation is attributed to the fact that the (ROP) is in general the resultant of two factors, which are the rotational speed stirring action and the (WOB) piercing action. Based on that no (ROP) will be achieved, no matter how high is the rotational speed, without applying (WOB) and vice versa. And by relying on these facts it can be concluded that increment in one of these two factors will have a positive influence on the other factor's effect on the (ROP).

Another point to be mentioned is that the rate of penetration (ROP), in general, decreases with depth. The rates of penetration (ROP) decrement percentage with depth from Figure (10, 13, and 16) were as in table (3) in Appendix (**B**). And this decrement in (ROP) is the result of the decrement in rotational speed, as a consequence of higher drag forces due to accumulative increment in compaction.

Finally, the average values of the power consumption (Watt) from Figure (11, 14, and 17) were as in table (4) in Appendix (**B**).

For the power consumption it should be reminded here that it corresponds to the actual rotational speed not the preset one since constant torque was used in this thesis. By examining the power consumption curves it can be seen that the power consumption increases as the rotational speed increases, with a decrement in that increment which might be physically ascribed to having higher inertia.

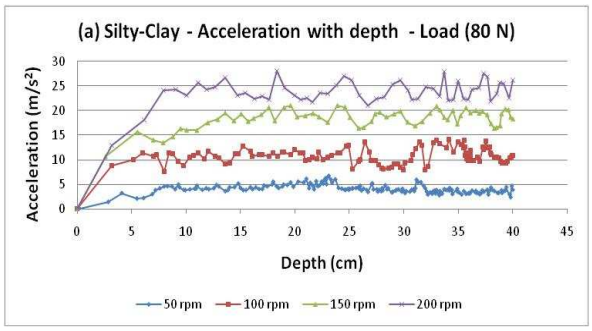

Fig. 9. Acceleration with depth.

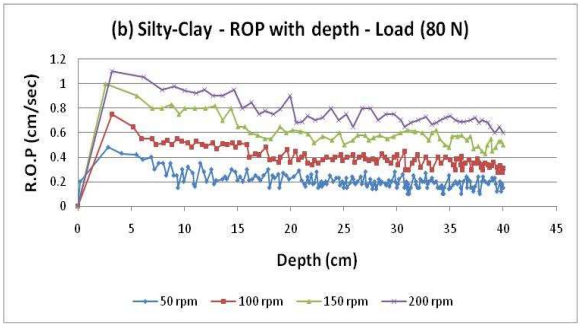

Fig. 10. Rate of penetration with depth.

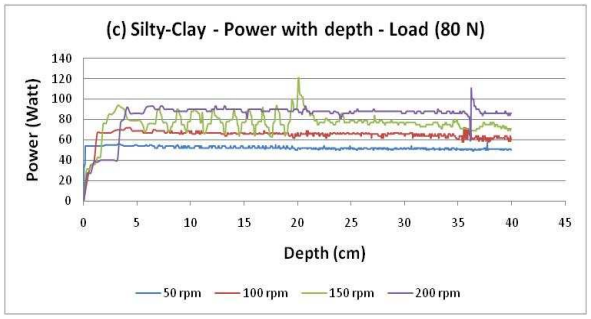

Fig. 11. Power with depth.

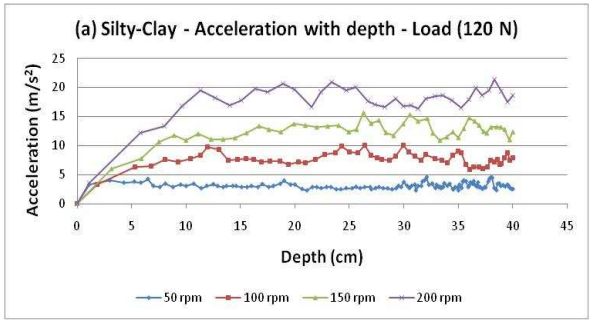

Fig. 12. Acceleration with depth.

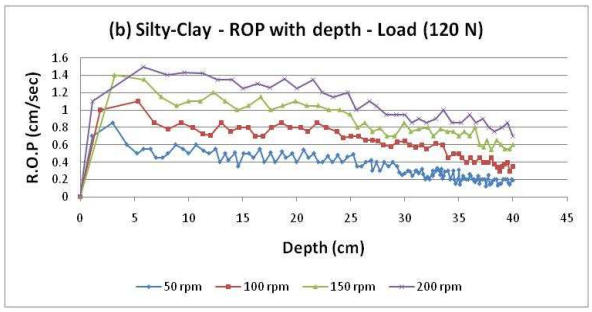

Fig. 13. Rate of penetration with depth.

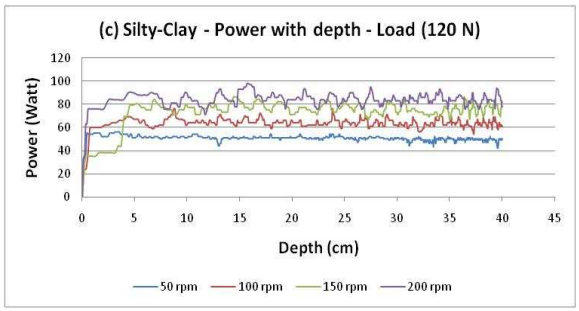

Fig. 14. Power with depth.

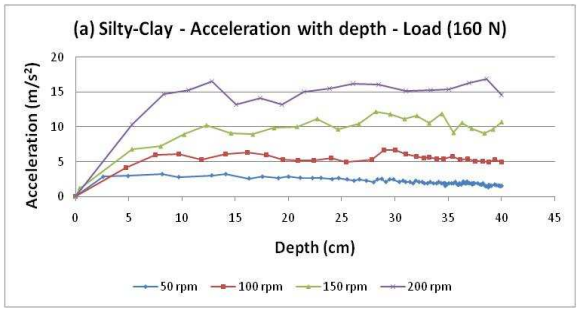

Fig. 15. Acceleration with depth.

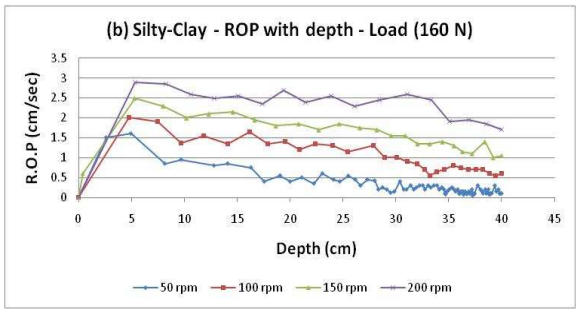

Fig. 16. Rate of penetration with depth.

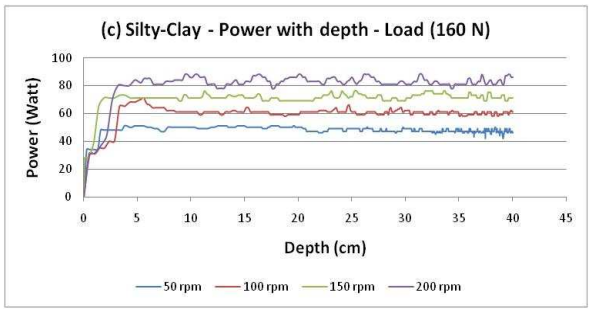

Fig. 17. Power with depth.

7.2.2. Sand

For the second soil sample (Sand), the average values of the vibration acceleration levels (m/s^2) from Figure (18, 21, and 24) were as in table (5) in Appendix (**B**).

Based on the revealed data, it can be said that vibration acceleration levels increase as the rotational speed increases. It also can be noticed that the vibration acceleration levels decrease as the weight on bit (WOB) increases. In general the vibration acceleration levels were higher than those encountered in silty-clay soil by (16.58%). Vibration acceleration levels decrement increases as the (WOB) and the rotational speed increase. All of the above mentioned observations can be attributed to the same factors that were mentioned in the silty-clay soil.

The average values of the rate of penetration (ROP) (cm/sec) from Figure (19, 22, and 25) were as in table (6) in Appendix (**B**).

In reference to table (9), it can be stated that higher rotational speed means higher rates of penetration (ROP). The rate of penetration (ROP) is seemed to be affected by the (WOB) in the same way that it did by the rotational speed and the higher the (WOB) is, the higher the (ROP) will be, but that's not completely practical due to the fact that (ROP) will keep increasing with the (WOB) up to a certain point, namely the founder point. After that point increasing the (WOB) will has adverse effect on the (ROP). It is worthy to mention that the sand soil has the higher rate of penetration in comparison to the silty-clay soil by (97.88%). The rate of penetration (ROP) increment increases as the (WOB) and the rotational speed increase. Another point to be mentioned is that the rate of penetration (ROP), in general, decreases with depth. The rates of penetration (ROP) decrement percentage with depth from Figure (19, 22, and 25) were as in table (7) in Appendix (**B**). All of the above mentioned observations can be attributed to the

same factors that were mentioned in the silty-clay soil.

Finally, the average values of the power consumption (Watt) from Figure (20, 23, and 26) were as in table (8) in Appendix (**B**).

By examining the power consumption curves it can be seen that the power consumption increases as the rotational speed increases, with a decrement in that increment which might be physically ascribed to having higher inertia.

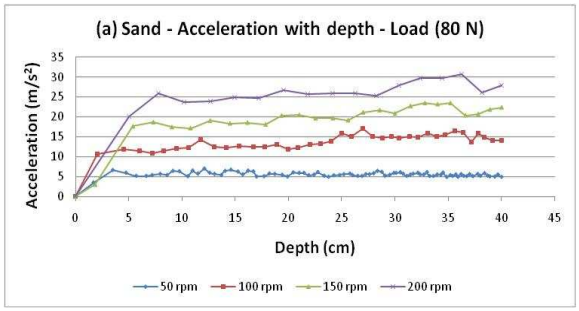

Fig. 18. Acceleration with depth.

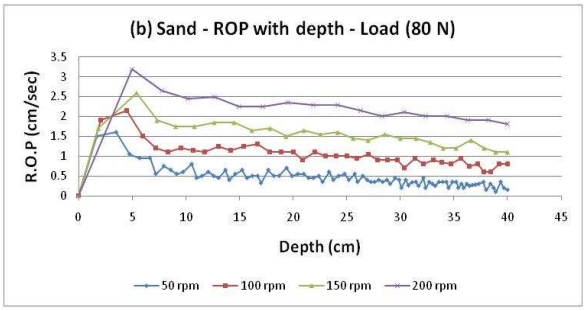

Fig. 19. Rate of penetration with dept.

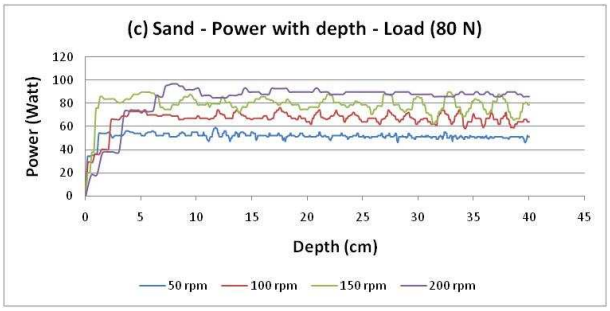

Fig. 20. Power with depth.

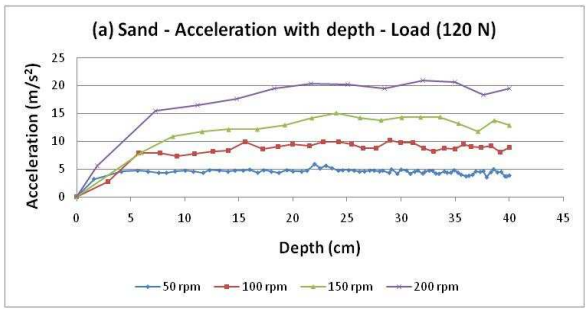

Fig. 21. Acceleration with depth.

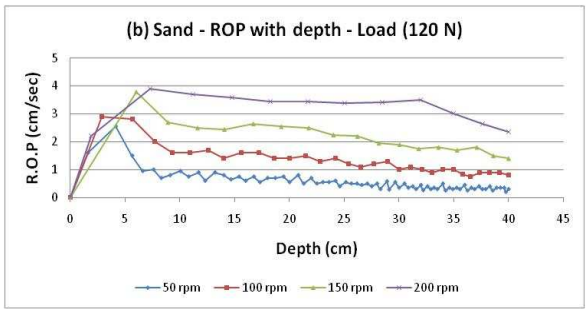

Fig. 22. Rate of penetration with depth.

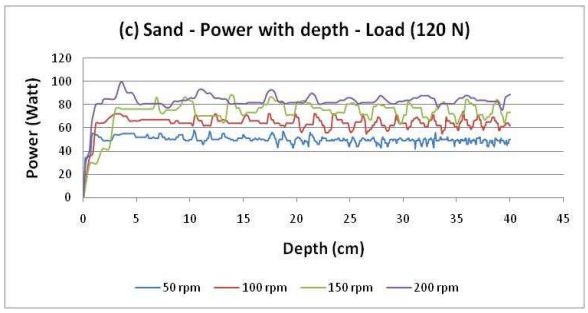

Fig. 23. Power with depth.

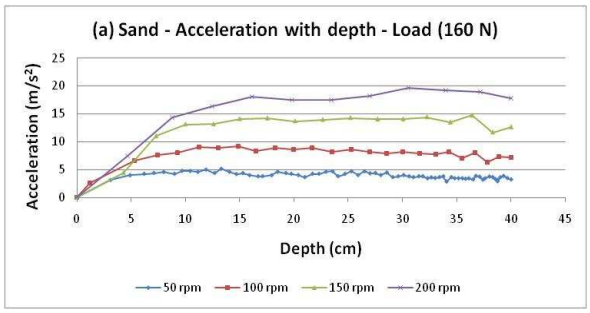

Fig. 24. Acceleration with depth.

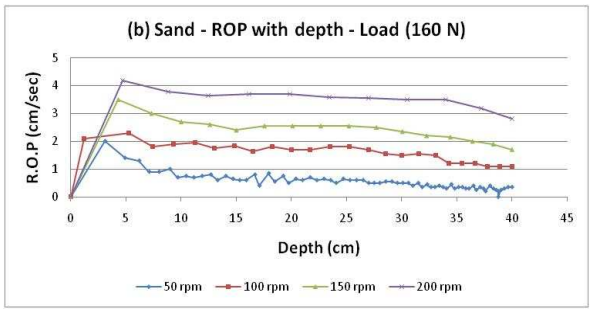

Fig. 25. Rate of penetration with dept.

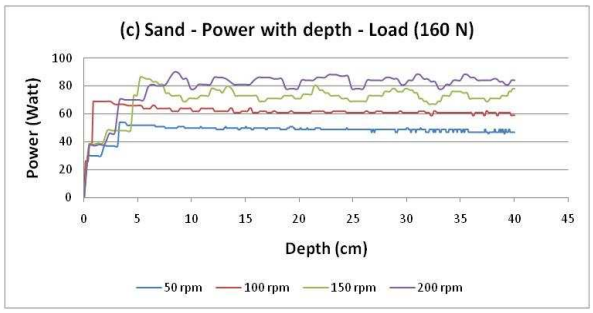

Fig. 26. Power with depth.

7.2.3. River Sand

For the final soil sample (River Sand), the average values of the vibration acceleration levels (m/s^2) from Figure (27, 30, and 33) were as in table (9) in Appendix (**B**).

Based on the revealed data, it can be said that vibration acceleration levels increase as the rotational speed increases. It also can be noticed that the vibration acceleration levels decrease as the weight on bit (WOB) increases. In general the vibration acceleration levels were lower than those in the sand and silty-clay soil by (25.53 % and 13.19 %) respectively. Vibration acceleration levels decrement increases as the (WOB) and the rotational speed increase. All of the above mentioned observations can be attributed to the same factors that were mentioned in the silty-clay soil.

The average values of the rate of penetration (ROP) (cm/sec) from Figure (28, 31, and 34) were as in table (10) in Appendix (**B**).

In reference to table (10), it can be stated that higher rotational speed means higher rates of penetration (ROP). The rate of penetration (ROP) is seemed to be affected by the (WOB) in the same way that it did by the rotational speed and the higher the (WOB) is, the higher the (ROP) will be, but that's not completely practical due to the fact that (ROP) will keep increasing with the (WOB) up to a certain point, namely the founder point. After that point increasing the (WOB) will has adverse effect on the (ROP). It is worthy to mention that the river sand soil has a higher rate of penetration than that of the silty-clay by (80.57 %) and lower than that of the sand by (8.75 %). The rate of penetration (ROP) increment increases as the (WOB) and the rotational speed increase. Another point to be mentioned is that the rate of penetration (ROP), in general, decreases with depth. The rates of penetration (ROP) decrement percentage with depth from Figure (28, 31, and 34) were as in table (11) in Appendix (**B**). All of the above mentioned observations can be attributed to the same factors that were mentioned in the silty-clay soil.

Finally, the average values of the power consumption (Watt) from Figure (29, 32, and 35) were as in table (12) in Appendix (**B**).

By examining the power consumption curves it can be seen that the power consumption increases as the rotational speed increases, with a decrement in that increment which might be physically ascribed to having higher inertia.

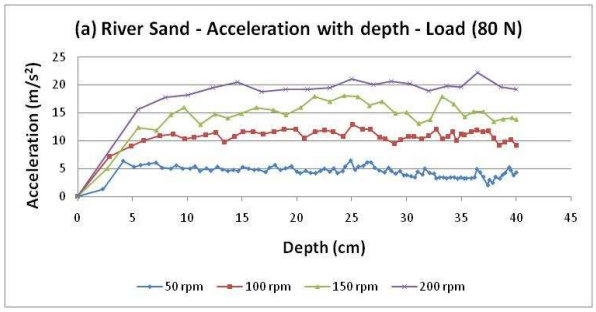

Fig. 27. Acceleration with depth.

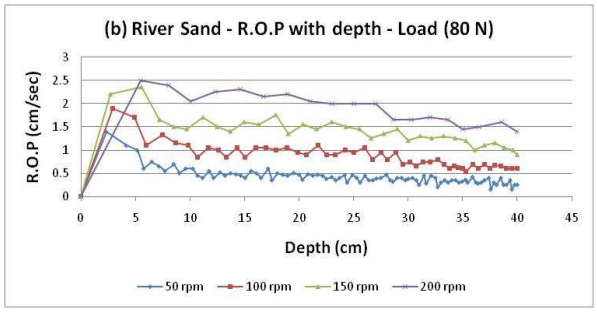

Fig. 28. Rate of penetration with depth.

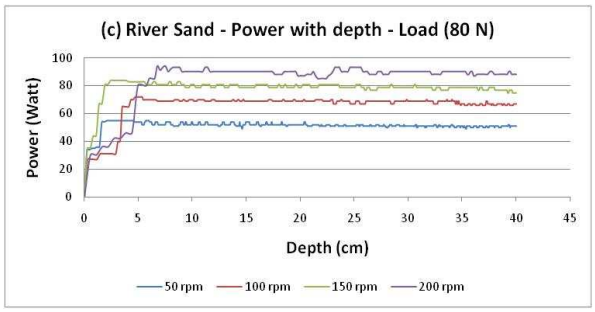

Fig. 29. Power with depth.

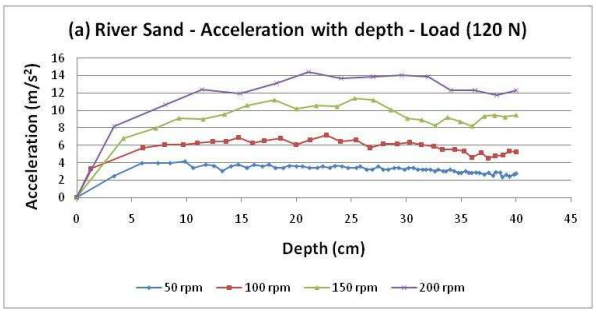

Fig. 30. Acceleration with depth.

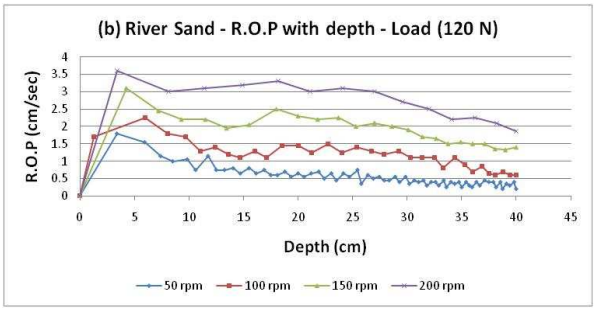

Fig. 31. Rate of penetration with depth.

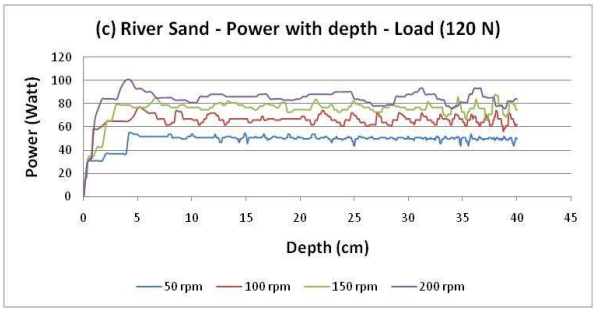

Fig. 32. Power with depth.

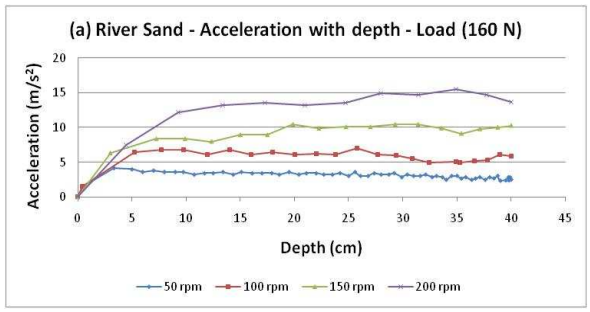

Fig. 33. Acceleration with depth.

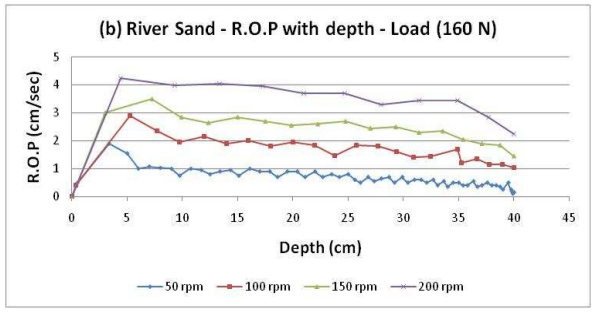

Fig. 34. Rate of penetration with depth.

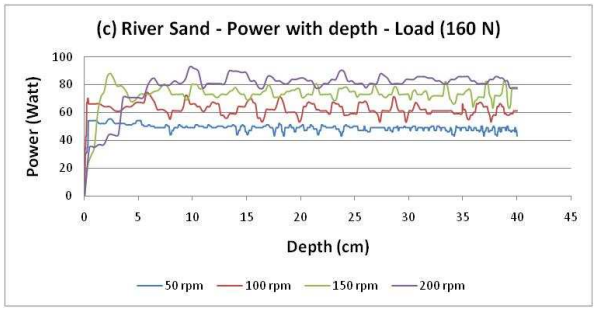

Fig. 35. Power with depth.

7.2.4. Free-Run (Idle Run)

In order to calculate the loads at the drill-bit inserts, establishing the power consumption curves for the free-run (idle run i.e. drilling with no contact between the drilling tool and the soil) was essential, so that the drilling power can be calculated by finding the difference between the steady state portion of the power consumption curves when drilling in the soil and outside the soil (i.e. the free-run).

The average values of the power consumption (Watt) were as follows in table (2) below:

Table 2,
Power Consumption (Watt).

	Load (80 N)	Load (120 N)	Load (160 N)
50 rpm	58.6	57.5	56.4
100 rpm	78.8	78.2	77.4
150 rpm	96	95.3	94.8
200 rpm	108.7	108.5	108.3

7.3. Results Verification

As mentioned previously ANSYS Workbench software (the 14.0 release) was used to verify the experimental results, and that's was accomplished by reliance on power consumption curves to calculate the drag force, that encounter the bit inserts, at the intervals of two centimeters and by using the supports stiffness values that had already been calculated previously by adapting Beam Deflection formula, as the input to the ANSYS. Additionally, twenty AutoCAD 2009 geometries due to the movement of the drill-string relative to the supports as the drilling operation proceeds forehead, which were also exported to the ANSYS. The deviation percentage was calculated by finding the average value of the trend lines of the numerical and actual acceleration curves, figure (1) – (12) in appendix (C), as follows in table (3) below:

$$Deviation\ (\%) = \left(\frac{numerical\ acc. - actual\ acc.}{actual\ acc.} * 100 \right)$$

Table 3
Results verification – Deviation percentage.

Load - 8 N			
r.p.m	**Actual acc.**	**Numerical acc.**	**Deviation percentage (%)**
50	4	3.7	7.5
100	10.5	9.5	9.52
150	15.5	17	9.68
200	22.5	21	6.67
Load - 12 N			
r.p.m	**Actual acc.**	**Theoritical acc.**	**Deviation percentage (%)**
50	3	2.7	10
100	7	7.5	7.14
150	12	13	8.33
200	16	17	6.25
Load - 16 N			
r.p.m	**Actual acc.**	**Theoritical acc.**	**Deviation percentage (%)**
50	2.4	2.2	8.33
100	5.1	5.6	9.8
150	8.5	9	5.88
200	14	15	7.14

8. Conclusions

When it comes to the conclusions and after observing the results illustrated by the charts that correlate the vibration acceleration, the rate of penetration and the power consumption curves with the depth of the borehole the following conclusions were pointed out. Part of them are special conclusions of the individual soil samples while the others are general conclusions, which are going to be mentioned later, and these conclusions are as follows:

1- Sand has stands out to be in the first place when it comes to the highest vibration acceleration levels (with an average acc. value of (13.097 m/s^2)), followed by silty-clay (11.234 m/s^2) and river sand (9.753 m/s^2) respectively.
2- For the rates of penetration sand also seemed to be the one with the highest penetration rate (with an average ROP of (1.786 cm/sec)) followed with close difference by the river sand (1.629 cm/sec) meanwhile silty-clay comes with the lowest ROP average (which was (0.902 cm/sec).

And now the general conclusions, which can be applied to all of the cases, are listed below:

3- The vibration acceleration levels increase as the rotational speed increases (provided that the implemented operating speed is away from the resonance zones).
4- The vibration acceleration levels decrease as the weight on bit (WOB) increases.
5- The vibration acceleration levels decrement increases as the (WOB) and the rotational speed increase.
6- Higher rotational speed means higher (ROP) since more excavation of the soil will be done.
7- The (ROP) will keep increasing with the (WOB) up to a certain point, the founder point, and after that point increasing the (WOB) will have adverse effect on the (ROP).
8- The rate of penetration (ROP) increment increases as the (WOB) and the rotational speed increase.
9- In general the rate of penetration (ROP) decreases with depth.

Finally, from the numerical analysis of the smaller and the larger drill bit models it was available to come up with the following:

10- It was observed that for the same conditions (soil type, rotational speed, and WOB) smaller drill bit diameter means higher vibration acceleration levels.

Notation

A Area of the transversal section (m^2)
E Young's modulus (pa)
G Shear modulus (pa)
g Gravitational acceleration (m/s^2)
H Strain energy (N.m)
H_s Simplified strain energy (N.m)
$\boldsymbol{I}$ Tensor of inertia (m^4)
K Kinetic energy (N.m)
u Displacement in x-direction (m)
v Displacement in y-direction (m)
w Displacement in z-direction (m)

Greek Letters

ρ Density (kg/m^3)
θ_x Rotation about x-axis (rad)
θ_y Rotation about y-axis (rad)
θ_z Rotation about z-axis (rad)

9. References

[1] R. W. Tucker and C. Wang, "An Integrated Model for Drill-String Dynamics", Article, 2000.

[2] D. K. Ashley, X. M. McNary, and J. C. Tomlinson, "Extending BHA Life with Multi-Axis Vibration Measurements", Paper (Society of Petroleum Engineers), 2001.

[3] M. W. Gui, M.ASCE, K. Soga, M. D. Bolton, and J. P. Hamelin, "Instrumented Borehole Drilling for Subsurface Investigation", Paper (Journal of Geotechnical and Geoenvironmental Engineers), 2002.

[4] R. I. Leine, D. H. van Campen, and W. J. G. Keultjes, "Stick-Slip Whirl Interaction in Drillstring Dynamics", Paper (Journal of Vibration and Acoustics), 2002.

[5] M.P.M. Hendriks, "Analysis of Torsional and Lateral Vibrations in an Experimental Drill-String Set-Up", Master thesis, 2004.

[6] Nenad Mihajlovic, "Torsional and Lateral Vibrations in Flexible Rotor Systems with Friction", Ph.D. thesis, 2005.

[7] Marcelo T. Piovan and Rubens Sampaio, "Non Linear Model for Coupled Vibrations of Drill-Strings", Paper, 2006.

[8] Hamed Moradi, Mohammad Motamedi, and Firooz Bakhtiari-Nejad, "Suppression of Bending Vibration in Drilling Process via a Tunable Vibration Absorber", Paper (16th International Congress on Sound and Vibration ICSV), 2009.

[9] Thiago Gamboa Ritto, "Numerical Analysis of the Nonlinear Dynamics of a Drill-String with Uncertainty Modeling", Ph.D. thesis, 2010.

[10] Chien-Min Liao, "Experimental and Numerical Studies of Drill-String Dynamics", Ph.D. thesis, 2011.

[11] Jerome Rajnauth, PhD and Tennyson Jagai, PhD, "Reduce Torsional Vibration and Improve Drilling operations", Paper (International Journal of Applied Science and Technology), 2012.

[12] Richard Duff, "An Experimental and Computational Investigation of Rotating Flexible Shaft System Dynamics in Rotary Drilling Assemblies for Down Hole Drilling Vibration Mitigation", Ph.D. thesis, 2013.

[13] M. Lalanne and G. Ferraris, John Wiley and Sons, Chichester, West Sussex, England, named "Rotor-dynamics Prediction in Engineering", 1990.

[14] M.A. Trindade, C. Wolter, and R. Sampaio, "Karhunen-loeve Decomposition of Coupled Axial/Vending Vibrations of Beams Subject to Impacts", Journal of Sound and Vibration, 2005.

Appendix (A)

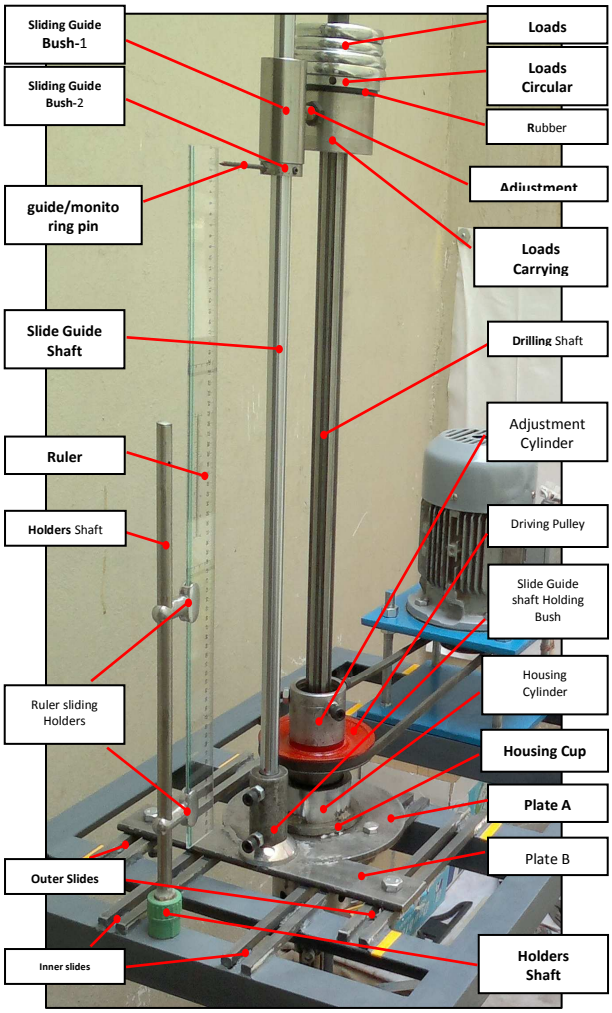

Fig. 1. the drill-string (drilling core) – upper parts.

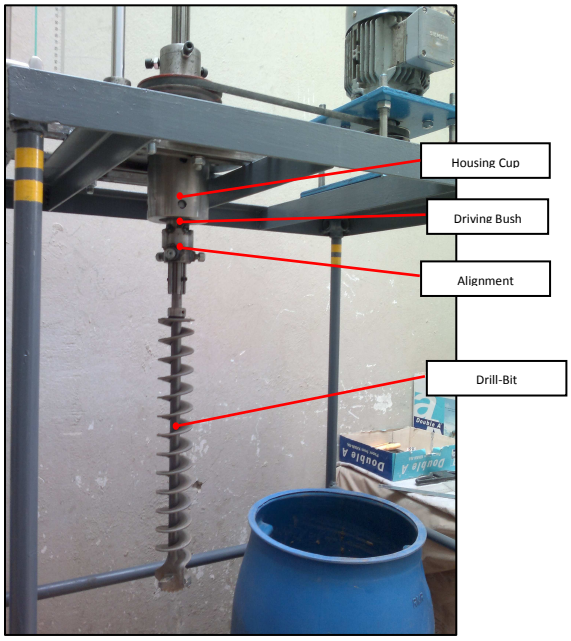

Fig. 2. the drill-string (drilling core) – lower parts.

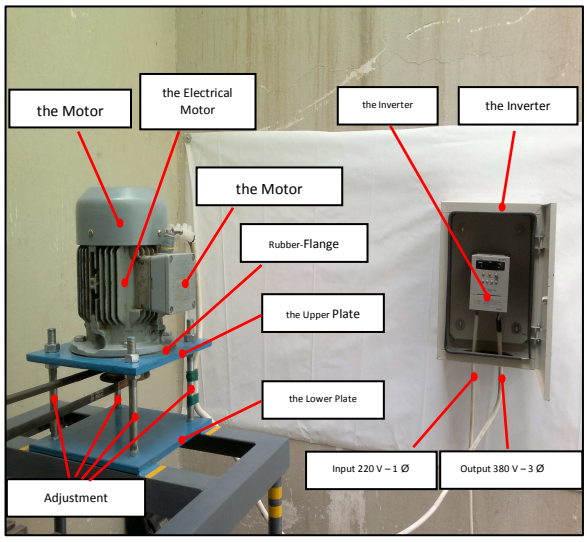

Fig. 3. the electrical motor and the inverter

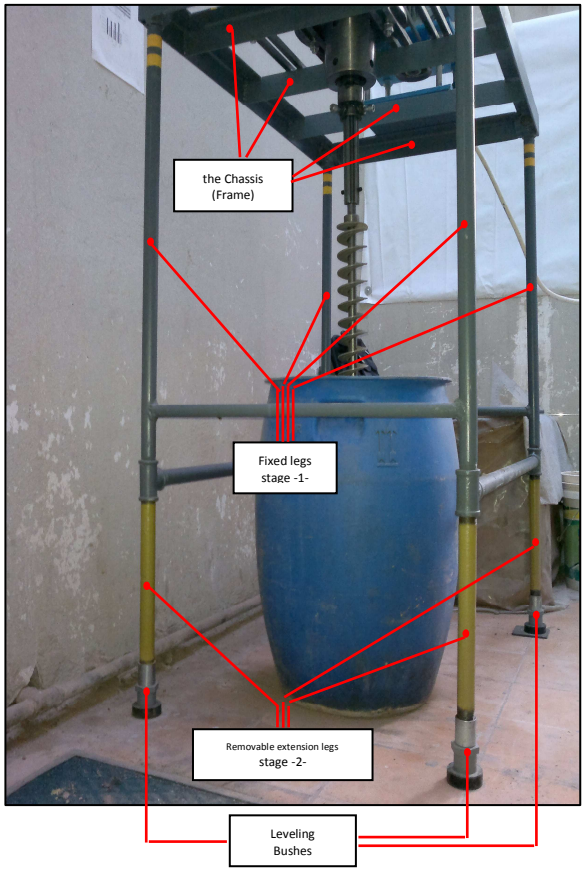

Fig. 4. the chassis (frame) – side view.

Appendix (B)

1. Silty- Clay

Table 1,
Vibration Acceleration Levels (m/s^2) & variation percentage.

Vibration Acceleration Levels (m/s^2) & variation percentage					
	Load (80 N)		Load (120 N)		Load (160 N)
50 rpm	4.35	-28.3 %	3.12	-29.8 %	2.19
	+154.7 %		+152.2 %		+161.6 %
100 rpm	11.08	-29 %	7.87	-27.2 %	5.73
	+79.4 %		+63.3 %		+83.8 %
150 rpm	19.88	-35.4 %	12.85	-18.1 %	10.53
	+18.2 %		+43.7 %		+44.7 %
200 rpm	23.5	-21.4 %	18.47	-17.5 %	15.24

Table 2,
Rates of Penetration ROP (cm/sec) & variation percentage.

Rates of Penetration ROP (cm/sec) & variation percentage					
	Load (80 N)		Load (120 N)		Load (160 N)
50 rpm	0.225	+48 %	0.333	+42.9 %	0.476
	+52 %		+110.8 %		+189.7 %
100 rpm	0.342	+105.3 %	0.702	+96.4 %	1.379
	+88.6 %		+23.9 %		+20.9 %
150 rpm	0.645	+34.9 %	0.870	+91.6 %	1.667
	+17.1 %		+24.3 %		+41.2 %
200 rpm	0.755	+43.2 %	1.081	+117.7 %	2.353

Table 3,
Rates of Penetration (ROP) decrement percentage.

Rates of Penetration (ROP) decrement percentage			
	Load (80 N)	Load (120 N)	Load (160 N)
50 rpm	23.4 %	37.9 %	15 %
100 rpm	26.3 %	31.4 %	33.1 %
150 rpm	32.7 %	32.5 %	48.3 %
200 rpm	32 %	45 %	70 %

Table 4,
Power Consumption (Watt).

Power Consumption (Watt)			
	Load (80 N)	Load (120 N)	Load (160 N)
50 rpm	51.67	50.02	47.55
100 rpm	65.35	63.96	60.69
150 rpm	77.14	76	71.73
200 rpm	87.82	84.42	83.23

2. Sand

Table 5,
Vibration Acceleration Levels (m/s^2) & variation percentage.

Vibration Acceleration Levels (m/s^2) & variation percentage					
	Load (80 N)		Load (120 N)		Load (160 N)
50 rpm	5.69	-17.9 %	4.67	-12.6 %	4.08
	+145 %		+91.2 %		+104.7 %
100 rpm	13.94	-35.9 %	8.93	-6.5 %	8.35
	+44.5 %		+52 %		+66 %
150 rpm	20.15	-32.7 %	13.57	+2.1 %	13.86
	+31.5 %		+42.3 %		+30.7 %
200 rpm	26.49	-27.1 %	19.31	-6.2 %	18.12

Table 6,
Rates of Penetration ROP (cm/sec) & variation percentage.

Rates of Penetration ROP (cm/sec) & variation percentage					
	Load (80 N)		Load (120 N)		Load (160 N)
50 rpm	0.471	+18 %	0.556	+2.7 %	0.571
	+123.6 %		+139.7 %		+191.9 %
100 rpm	1.053	+26.6 %	1.333	+25.1 %	1.667
	+51.9 %		+76.5 %		+50 %
150 rpm	1.6	+47.1 %	2.353	+6.2 %	2.5
	+47.1 %		+41.6 %		+45.4 %
200 rpm	2.353	+41.6 %	3.333	+9.1 %	3.636

Table 7,
Rates of Penetration (ROP) decrement percentage.

Rates of Penetration (ROP) decrement percentage			
	Load (80 N)	Load (120 N)	Load (160 N)
50 rpm	15 %	14.4 %	10.8 %
100 rpm	28.3 %	32 %	18.1 %
150 rpm	32.5 %	32.5 %	35 %
200 rpm	63.8 %	67.2 %	60 %

Table 8,
Power Consumption (Watt).

Power Consumption (Watt)			
	Load (80 N)	Load (120 N)	Load (160 N)
50 rpm	51.5	49.52	48.9
100 rpm	67.49	64.5	61.83
150 rpm	79.5	75.24	73.59
200 rpm	89.14	84.17	83.48

3. River sand

Table 9,
Vibration Acceleration Levels (m/s^2) & variation percentage.

Vibration Acceleration Levels (m/s^2) & variation percentage					
	Load (80 N)		Load (120 N)		Load (160 N)
50 rpm	4.64	26.9 %	3.39	5.3 %	3.21
	153.9 %		77.3 %		87.2 %
100 rpm	11.78	49 %	6.01	0 %	6.01
	30.2 %		75.7 %		57.2 %
150 rpm	15.34	31.2 %	10.56	10.5 %	9.45
	27.4 %		25 %		47 %
200 rpm	19.55	32.5 %	13.2	-5.2 %	13.89

Table 10,
Rates of Penetration ROP (cm/sec) & variation percentage.

Rates of Penetration ROP (cm/sec) & variation percentage					
	Load (80 N)		Load (120 N)		Load (160 N)
50 rpm	0.444	36.5 %	0.606	11.9 %	0.678
	83.8 %		106.3 %		168.1 %
100 rpm	0.816	53.2 %	1.25	45.4 %	1.818
	53.2 %		39.1 %		29.4 %
150 rpm	1.25	39.12 %	1.739	35.3 %	2.353
	68.4 %		64.3 %		54.5 %
200 rpm	2.105	35.7 %	2.857	27.3 %	3.636

Table 11,
Rates of Penetration ROP (cm/sec) & variation percentage.

Rates of Penetration (ROP) decrement percentage			
	Load (80 N)	Load (120 N)	Load (160 N)
50 rpm	25.4 %	22.4 %	20 %
100 rpm	26.3 %	28.3 %	27.1 %
150 rpm	45 %	59.7 %	33.1 %
200 rpm	48.8 %	65 %	55 %

Table 12,
Power Consumption (Watt).

Power Consumption (Watt)			
	Load (80 N)	Load (120 N)	Load (160 N)
50 rpm	51.57	50.52	48.48
100 rpm	68.51	66.36	62.14
150 rpm	79.33	76.95	73.68
200 rpm	89.5	84.84	83.31

Appendix (C)

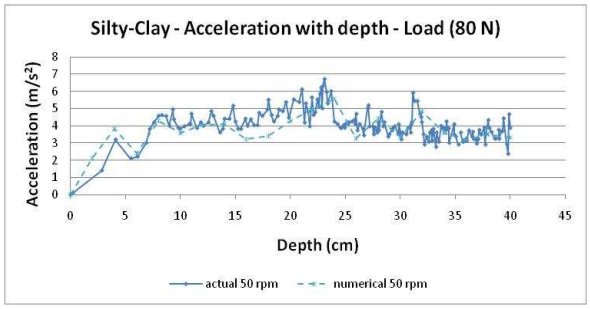

Fig. 1. Act. and Theo. Acc. With depth (80 N & 50 rpm)

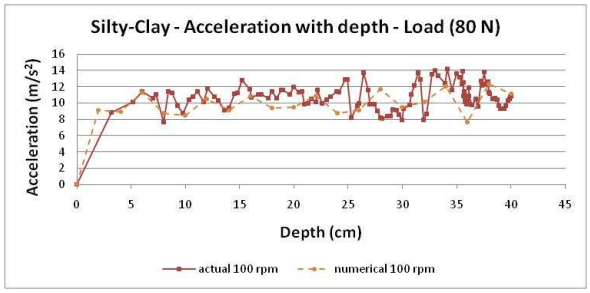

Fig. 2. Act. and Theo. Acc. With depth (80 N & 100 rpm)

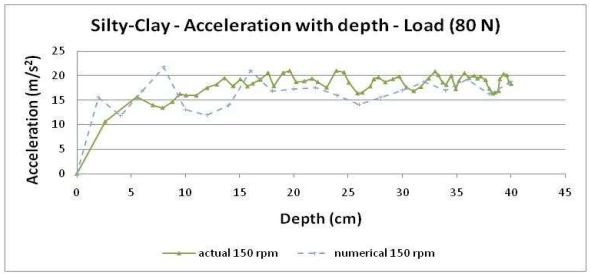

Fig. 3. Act. and Theo. Acc. With depth (80 N & 150 rpm)

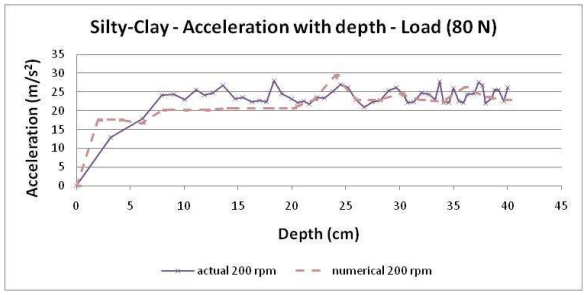

Fig. 4. Act. and Theo. Acc. With depth (80 N & 200 rpm)

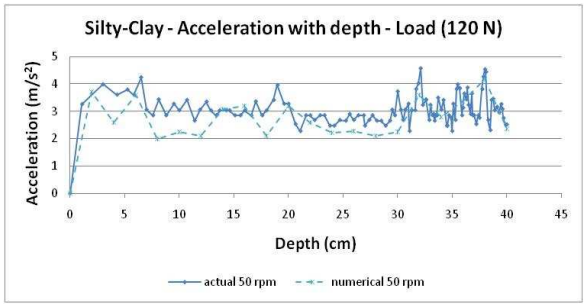

Fig. 5. Act. and Theo. Acc. With depth (120 N & 50 rpm)

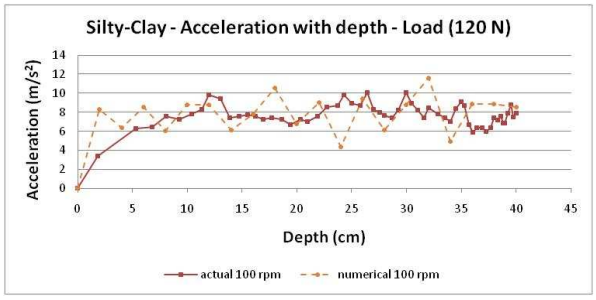

Fig. 6. Act. and Theo. Acc. With depth (120 N & 100 rpm)

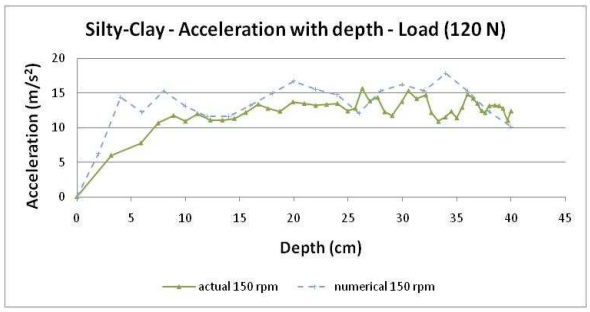

Fig. 7. Act. and Theo. Acc. With depth (120 N & 150 rpm)

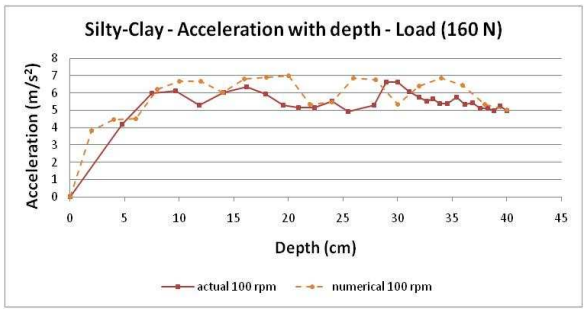

Fig. 10. Act. and Theo. Acc. With depth (160 N & 100 rpm)

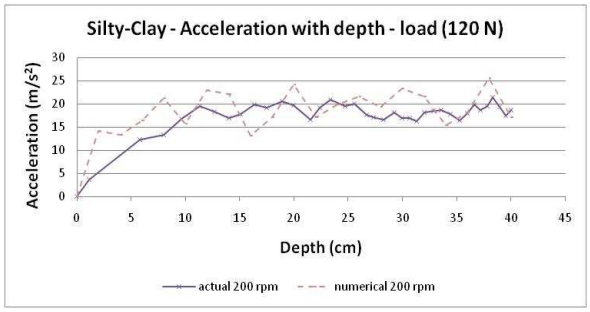

Fig. 8. Act. and Theo. Acc. With depth (120 N & 200 rpm)

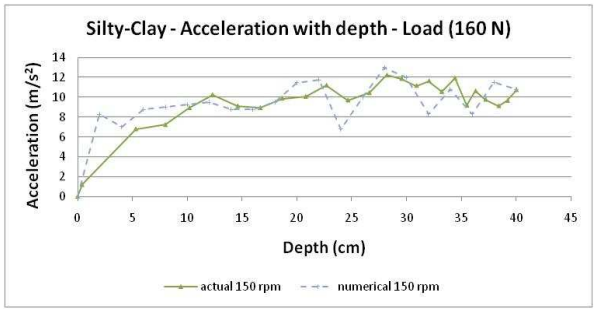

Fig. 11. Act. and Theo. Acc. With depth (160 N & 150 rpm)

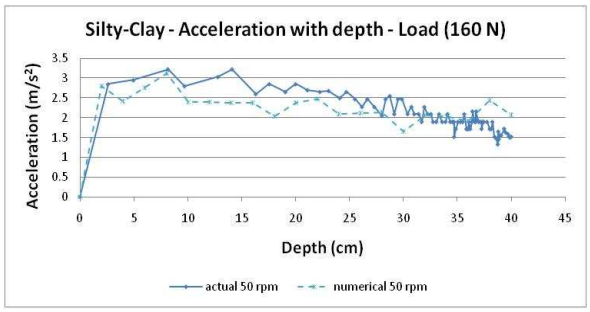

Fig. 9. Act. and Theo. Acc. With depth (160 N & 50 rpm)

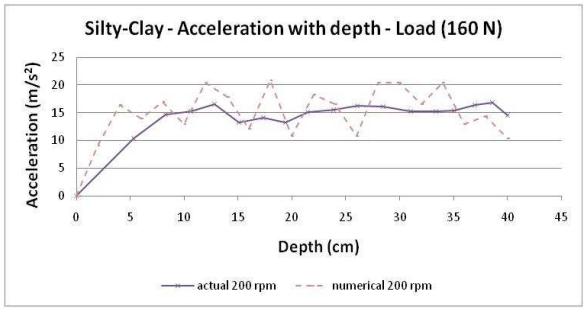

Fig. 12. Act. and Theo. Acc. With depth (160 N & 200 rpm)

Appendix (D)

Instruments Connection

The diagram below (Figure (1)) illustrates the position where the accelerometers were attached to the drill-string for measuring the vibration acceleration and how the instruments were connected to each other.

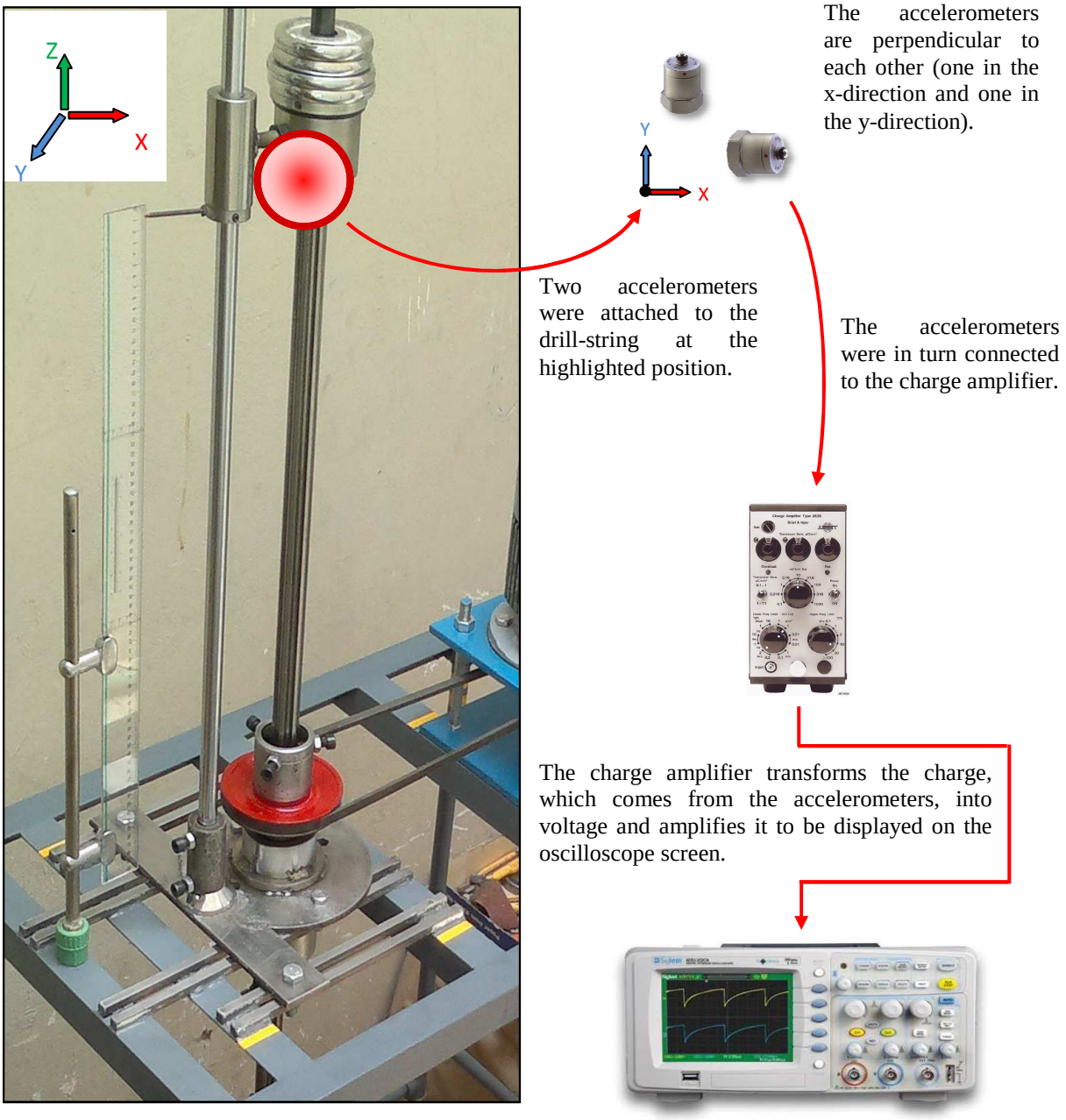

Fig. 1. Instruments connection diagram.

تأثير مُحتوى التُربة، مَقاييس الحَفر وقطر عُدة الحَفر على الإهتِزازات الحاصِلة في مَنظومة الحَفر

موفق علي توفيق* وفاء عبد سعود**

رامي صفاء علوان***

*،**،*** قسم هندسة المكائن والمعدات/ الجامعة التكنولوجية

*البريد الالكتروني: drmat19853@yahoo.com

**البريد الالكتروني: wafaabd_92@yahoo.com

***البريد الالكتروني: rami.safaa@yahoo.com

الخُلاصة

هذا البحث يُمثل دِراسة لتأثير نوع التُربة، مَقاييس الحَفر، وقُطر عُدة الحَفر على السُلوك الديناميكي الإهتزازي وتحليله في مِنصة الحَفر. ولهذا الغرض تم تصميم وبناء مِنصة حَفر مُختبرية لإجراء التجارب المُتعلقة بالجانب العَملي من البحث، حيث ان الجانب العَملي اشتمل على تشغيل عمود الحَفر في انواع مُختلفة من التُرب ذات خواص مُختلفة نِسبة الى اختِلاف حجم الحُبيبات، بسُرع دورانية مُختلفة، وبأحمال مُختلفة، وبالشكل الذي يُتيح رسم المُنحَنيات التي تربط تسارع الإهتزاز، مُعدل الإختراق (ROP) وإستهلاك الطاقة مع عُمق الحَفر.

فضلاً عن ذلك فقد تم استِخدام برنامج ال ANSYS Workbench (the 14.0 release) لمُحاكاة التجارب المُختبرية والتحقق من صِحتها، وكذلك فقد تم استِخدامه لتمثيل حالات نظرية اخرى باقطار مُختلفة لبريمة الحَفر.
